

Disorder-induced currents as signatures of chiral superconductivity

Madhuparna Karmakar^{1,*} and R. Ganesh^{2,†}

¹*Department of Physics, Indian Institute of Technology Madras, Chennai 600036, India*

²*The Institute of Mathematical Sciences, HBNI, C I T Campus, Chennai 600113, India*

(Dated: November 3, 2023)

Chiral superconductors are expected to carry a spontaneous, chiral and perpetual current along the sample edge. However, despite the availability of several candidate materials, such a current has not been observed in experiments. In this article, we suggest an alternative probe in the form of impurity-induced chiral currents. We first demonstrate that a single non-magnetic impurity induces an encircling chiral current. Its direction depends on the chirality of the order parameter and the sign of the impurity potential. Building on this observation, we consider the case of multiple impurities, e.g., realized as adatoms deposited on the surface of a candidate chiral superconductor. We contrast the response that is obtained in two cases: (a) when the impurities are all identical in sign and (b) when the impurities have mixed positive and negative signs. The former leads to coherent currents within the sample, arising from the fusion of individual current loops. The latter produces loops of random chirality that lead to incoherent local currents. These two scenarios can be distinguished by measuring the induced magnetic field using recent probes such as diamond NV centres. We argue that impurity-induced currents may be easier to observe than edge currents, as they can be tuned by varying impurity strength and concentration. We demonstrate these results using a toy model for $p_x \pm ip_y$ superconductivity on a square lattice. We develop an improved scheme for Bogoliubov deGennes (BdG) simulations where both the order parameter as well as the magnetic field are determined self-consistently.

I. INTRODUCTION

A superconductor is said to be chiral if it spontaneously breaks time reversal symmetry^{1,2}. Such states have long been known, starting with liquid He³ which is technically a superfluid and not a superconductor³. Interest in chiral superconductivity has grown alongside studies on non-superconducting time-reversal-breaking states such as quantum Hall systems. In both classes of systems, typical excitation spectra show non-trivial topology. This shared thread has motivated extensive studies into edge currents. Despite several experimental studies and theoretical refinements, such a current has hitherto not been observed in a chiral superconductor. This situation can be contrasted with the relatively quick detection of edge states in topological insulators⁴ and with the recent detection of an edge current in a topological non-chiral superconductor⁵. In this article, we propose measuring a different type of current – one induced by impurities. This provides a direct, observable and tunable manifestation of chirality.

Several materials have been proposed as candidates for chiral superconductivity. The most prominent is Sr₂RuO₄, long thought to be a $p + ip$ superconductor. However, experimental studies have proved inconclusive. Recent studies have revived this debate⁶. Chiral superconductivity has also been proposed to occur in heavy fermion materials⁷, SrPtAs⁸, highly doped graphene^{9,10} and transition metal dichalcogenides^{11,12}. In these materials, any evidence for chirality comes from bulk measurements such as μ SR or the Kerr effect. In some cases, scanning tunnelling probes have found in-gap states at edges¹³. However, an electrical current at an edge has not been observed so far^{14,15}.

In this backdrop, recent technologies to detect microscopic currents can break new ground. The most prominent of these uses nitrogen-vacancy (NV) centres – atomic defects within a diamond probe. A spectroscopic measurement of excitations at the defect conveys information about the local magnetic field¹⁶. As NV centres can operate over a wide temperature range and at nanometre separations from the sample, they can measure detailed field distributions. This has been used to map the spatial distribution of a current within graphene^{17,18}. With regard to edge currents of chiral superconductors, NV centres may succeed if they are sensitive enough to detect weak currents that were unobservable with earlier probes. However, edge currents may be unobservable due to deeper issues such as dissipation¹⁹, disorder^{20,21} and compensating magnetization textures²². Such hurdles cannot be circumvented easily as edges are simple objects with no tunable handles – atleast over coarse-grained length scales that are appropriate for mesoscopic probes. In this article, we describe an alternative signature where the magnitude and range of chiral currents can be tuned. We discuss signatures in magnetic field distributions that can be easily measured with probes such as NV centres.

II. TOY MODEL FOR CHIRAL SUPERCONDUCTIVITY

We consider a simple model with electrons hopping on a square lattice. The Hamiltonian is given by

$$H = -t \sum_{\sigma, \langle ij \rangle} \left\{ e^{i \frac{e}{\hbar} \mathcal{A}_{ij}} c_{i,\sigma}^\dagger c_{j,\sigma} + h.c. \right\} + H_{int}, \quad (1)$$

We restrict hoppings to nearest neighbours for simplicity. The hopping amplitude, t , sets the energy scale for the problem. Each hopping element carries a Peierls' phase that encodes the vector potential, with $\mathcal{A}_{ij} = \int_i^j \vec{A}(\mathbf{r}) \cdot d\mathbf{l}$. We have denoted the charge of the electron as e . Below, unless specified otherwise, we will set e/\hbar to unity. The vector potential here originates from supercurrents in the sample and not from an externally imposed magnetic field. Its precise form will be discussed below.

We choose an artificial interaction term designed to give rise to chiral superconductivity,

$$H_{int} = -g \sum_{\langle ij \rangle} \mathcal{D}_{ij}^\dagger \mathcal{D}_{ij}. \quad (2)$$

The sum runs over all nearest neighbour pairs of sites. The coupling constant, g , is taken to be positive. We introduce a two-site Cooper pair annihilation operator,

$$\mathcal{D}_{ij} = c_{i,\mu} (\sigma_3 i \sigma_2)_{\mu,\mu'} c_{j,\mu'} = \{c_{i,\uparrow} c_{j,\downarrow} + c_{i,\downarrow} c_{j,\uparrow}\}, \quad (3)$$

where the σ 's are Pauli matrices. While a generic triplet Cooper pair can contain three components with spin $m_z = -1, 0, 1$, we have only retained the the $m_z = 0$ component in \mathcal{D}_{ij} . In order to gain energy from the interaction term, the Cooper pair operator acquires a non-zero expectation value with $\langle \mathcal{D}_{ij} \rangle = \Delta_{ij}$, a complex scalar. However, this expectation value must satisfy certain constraints. From fermionic anticommutation relations, we see that $\Delta_{ij} = -\Delta_{ji}$. This signifies that the order parameter has p -wave symmetry, changing sign under a π -rotation. For instance, upon a π rotation about a bond centre, the bond direction changes from ij to ji so that the order parameter flips sign. Each site has four bonds emanating from it. In order to lower energy on each of these bonds, the order parameter naturally develops chiral $p_x \pm ip_y$ symmetry. Moving counterclockwise around a site, the phase of the order parameter increases or decreases by $\pi/2$ from one bond to the next.

A detailed study of this model can be found in Ref. 23. In summary, the system spontaneously chooses between one of two chiralities, i.e., between $p_x + ip_y$ and $p_x - ip_y$ character. Ordering introduces a quasiparticle gap, with the same spectrum for both chiralities in an infinite system. However, in the presence of an edge, we find a sharp signature that distinguishes the two chiralities. The quasiparticle spectrum hosts a mode within the bulk gap that propagates along the edge. The direction of propagation is determined by the chirality of the bulk order parameter. It is this mode that carries the edge current, providing a signature of chiral superconductivity. As a quasiparticle mode in a superconductor, this mode is a mixture of particle and hole components. As a consequence, it does not carry a quantized charge current – unlike an edge current in a Chern insulators.

A. Role of impurities

We now introduce impurities into the problem in the form of potentials on a certain fraction of sites. For simplicity, we assume that the amplitude of the potential is the same at each impurity site. As for the sign of the impurity potential, we consider two schemes: (i) correlated disorder – with every impurity carrying the same sign, and (ii) random disorder – with each impurity having a random sign. We represent these as

$$H_{corr.} = W \sum_{\{i\}} \sum_{\sigma} c_{i,\sigma}^\dagger c_{i,\sigma}, \quad (4)$$

$$H_{rand.} = W \sum_{\{i\}} \delta_i \sum_{\sigma} c_{i,\sigma}^\dagger c_{i,\sigma}. \quad (5)$$

In both cases, the sum over i runs over a randomly selected subset of sites. We consider the fraction of impurity sites to be a tunable parameter, η . In the random case, $\delta_i = \pm 1$ is an Ising-like random variable that is independently chosen at each impurity site. These two impurity schemes can be realized by placing a collection of adatoms on the surface of a chiral superconductor. If all adatoms are of the same type, this corresponds to the situation encoded in $H_{corr.}$. Here, the sign of the potential is decided by the relative electronegativity of the adatom with respect to the substrate. On the same lines, deposition of two species of adatoms can realize $H_{rand.}$.

III. BOGOLIUBOV DEGENNES SIMULATIONS

We consider the system on a $L \times L$ lattice with periodic boundary conditions. We perform a mean-field decomposition of the interaction term in Eq. 2, by defining bond variables $\Delta_{ij} \equiv \langle \mathcal{D}_{ij} \rangle$. This allows us to write the Hamiltonian as a quadratic form with

$$H = \Psi^\dagger M \Psi, \quad (6)$$

where $\Psi = \{\dots c_{i,\uparrow} \dots c_{i,\downarrow}^\dagger \dots\}^T$. The $2L \times 2L$ Hamiltonian matrix can be written as

$$M = \begin{pmatrix} K(t, \vec{A}, W) & P(\Delta_{mn}) \\ P(\Delta_{mn})^\dagger & -K(t, \vec{A}, W)^T \end{pmatrix}. \quad (7)$$

The diagonal blocks, $K(t, \vec{A}, W)$ encode hoppings with Peierls' phases and impurity potentials. The off-diagonal blocks contain the mean-fields, Δ_{mn} for each pair of neighbouring sites (m, n) . In typical Bogoliubov de-Gennes (BdG) calculations, the superconducting order parameters are determined using $\Delta_{mn} \equiv \langle \mathcal{D}_{mn} \rangle$. At the same time, the vector potential is either ignored or assumed to be fixed by a strong (non-self-consistent) external field. In this article, we present an improved BdG scheme where the vector potential is also determined self-consistently.

To determine the vector potential, we note that each bond carries a current. By adapting the arguments in

Ref. 24, we define the bond current operator as $\hat{J}_{mn} = \partial\hat{H}/\partial\mathcal{A}_{mn}$, where \hat{H} is the full Hamiltonian and (m, n) represents a pair of neighbouring sites. We obtain

$$\hat{J}_{mn} \approx \frac{e}{\hbar} \hat{\mathcal{J}}_{mn} + \left(\frac{e}{\hbar}\right)^2 \hat{\mathcal{K}}_{mn} \mathcal{A}_{mn} + \mathcal{O}(\mathcal{A}_{mn}^2),$$

where

$$\hat{\mathcal{J}}_{mn} = t \sum_{\sigma} \langle \{ic_{m,\sigma}^\dagger c_{n,\sigma} - ic_{n,\sigma}^\dagger c_{m,\sigma}\} \rangle, \quad (8)$$

$$\hat{\mathcal{K}}_{mn} = t \sum_{\sigma} \langle \{c_{m,\sigma}^\dagger c_{n,\sigma} + c_{n,\sigma}^\dagger c_{m,\sigma}\} \rangle. \quad (9)$$

In the absence of a vector potential, $\hat{\mathcal{J}}_{mn}$ and $\hat{\mathcal{K}}_{mn}$ would encode the bond current and the bond energy respectively. We neglect $\mathcal{O}(\mathcal{A}_{mn}^2)$ terms here, assuming that \mathcal{A}_{mn} is small on every bond. This is justified in the limit of weak disorder. Currents in our system are induced solely by disorder. Weak disorder will give rise to weak currents and, in turn, to a weak vector potential. The current expression in Eq. 8 requires numerical coefficients that are proportional to e/\hbar and $(e/\hbar)^2$. In our calculational scheme, we replace these with arbitrary numbers, taking $\langle \hat{J}_{mn} \rangle \approx \langle \hat{\mathcal{J}}_{mn} \rangle + 0.01 \langle \hat{\mathcal{K}}_{mn} \rangle \mathcal{A}_{mn}$. In a more realistic calculation, these coefficients can be fixed using precise values of e , \hbar and the hopping integrals.

We next discuss the vector potential induced by the bond currents of Eq. 9. Assuming the Coulomb gauge condition ($\vec{\nabla} \cdot \vec{A} = 0$), a closed form expression can be derived for the vector potential induced by a set of static source currents,

$$\vec{A}(\mathbf{r}) = \frac{\mu_0}{4\pi} \int d^2 r' \frac{\vec{J}(r')}{|\mathbf{r} - \mathbf{r}'|}. \quad (10)$$

This relation follows from the Biot-Savart law and the integral solution to the Poisson's equation. We adapt this equation to our lattice problem using

$$\mathcal{A}_{ij} = \frac{\mu_0}{4\pi} \left[\sum_{\{kl\} \parallel \{ij\}} \frac{J_{kl}}{|\mathbf{R}_{kl} - \mathbf{R}_{ij}|} + \frac{J_{ij}}{\delta\ell} \right]. \quad (11)$$

For concreteness, we set $\mu_0/4\pi = 0.1$ in our calculations. Here, the index ij represents the reference bond where the vector potential is to be determined. The position of the centre of the bond is denoted as \mathbf{R}_{ij} . The sum runs over kl , all other bonds that are parallel to ij , i.e., if ij is a bond in the x -direction, kl runs over all x -bonds except ij . The centre of each of these bonds is denoted as \mathbf{R}_{kl} . We calculate inter-bond distances ($|\mathbf{R}_{kl} - \mathbf{R}_{ij}|$) assuming that the lattice constant is unity. The last term in the above equation represents the contribution from the very same bond, ij . Naively this represents a singular contribution as the source current and the target bond coincide, i.e., $|\mathbf{R}_{kl} - \mathbf{R}_{ij}|$ vanishes. However, this contribution will be cutoff by microscopic length scales, e.g., the bond current may be carried via orbital channels

that are slightly displaced from the bond vector. We phenomenologically model such effects using a cutoff length scale denoted as $\delta\ell$. In the calculations discussed below, we use $\delta\ell = 0.1$.

We obtain the order parameters and the vector potential self-consistently. Starting with random values of Δ_{ij} 's and \mathcal{A}_{ij} 's, we obtain a new set of values as described above. We iterate this process until self-consistency is achieved. The calculations are carried out while respecting periodic boundary conditions. Each distance ($\mathbf{R}_{ij} - \mathbf{R}_{kl}$) in Eq. 11 is chosen in accordance with the periodicity of the lattice. For example, two bonds are placed in neighbouring unit cells if that gives the lowest distance between them. We note that our approach does not give consistent results with open boundary conditions. In the presence of an edge, the vector potential outside the sample cannot be taken into account. Technically, this prevents us from ensuring $\vec{\nabla} \cdot \vec{A} = 0$, a necessary condition for the use of Eq. 10.

We emphasize that our scheme is an improvement over standard BdG approaches. As the vector potential is determined self-consistently, our approach allows for ‘screening’ currents. These can be viewed as a manifestation of the Meissner effect, with any magnetic field diminished by counter-currents that naturally arise in a superconductor. In the context of Sr_2RuO_4 , it has been shown edge currents are indeed strongly screened^{25,26}.

IV. RESPONSE TO A SINGLE IMPURITY

We first consider the case of a single impurity in our chiral superconductor. Before discussing our results, we review some basic ideas. Chirality allows for a spontaneous local current that circulates around an impurity. This can be understood as follows. We imagine a hole cut into the superconductor. As the superconductor is chiral, it hosts a chiral boundary current that propagates along the edge. The hole can be replaced by a plateau-shaped potential which repels electrons from the interior region. We now imagine shrinking the radius of the ‘hole’, with the boundary current smoothly deforming to cling to the shrinking perimeter. When the radius approaches zero, we are left with a point-like potential. In this limit, the boundary current takes the form of a local current encircling the impurity. The current is no longer quantized as we can now have scattering between opposite edges of the hole. Nevertheless, we expect a non-zero current strength. Based on similar arguments, an impurity-induced current has been studied in a Chern insulator²⁷.

Before presenting results on impurity response, we discuss chirality in our mean-field solutions. In clean as well as in disordered systems, we find two mean-field solutions that correspond to a choice of chiralities. They can be understood as $\Delta_x \pm i\Delta_y$ configurations: the order parameters on the x and y bonds differ by a phase of $\pm\pi/2$. In all our calculations, we find that the system picks one

global chirality with no domain walls separating regions of differing chirality. For concreteness, in the discussion below, we restrict our attention to solutions of the form $\Delta_x + i\Delta_y$.

Our results for the response to a single impurity are shown in Fig. 1. The panels on the left show the order parameter amplitude on x bonds. The panels in the second column show amplitudes on the y bonds. Here, $\Delta_{x/y}^i$ is the order parameter on the bond emanating from site i in the x/y -direction. In these plots, we see that the impurity creates a local distortion in order parameters. In addition, magnetic fields are generated as shown in the third column. The fields (fluxes, to be more precise) are defined on plaquettes, given by the sum of Peierls' phases (vector potentials) along four bonds. The field is strongest at the plaquettes that are immediately adjacent to the impurity, oscillating as we move further. Crucially, the direction of magnetic flux on a given plaquette is determined by the sign of the impurity potential. This field originates from a current that circulates around the impurity, as shown in the panels on the right. The current is only appreciable on bonds that are close to the impurity. For a given background chirality, the direction of the current loop is set by the sign of the impurity potential.

In Fig. 2, we show the profile generated by a single impurity. We show the current induced on neighbouring bonds, the resulting vector potential and the magnetic field. We see that the response is highly localized, with the responses decaying sharply as we move away from the impurity. This figure is to be compared with well-known results on edge currents, e.g., in Ref. 26. Our problem is fundamentally different as it lacks the translational symmetry of a linear edge. Nevertheless, the profiles show some degree of similarity. This comparison also brings out an advantage of impurities over edges. An edge is a sharply defined feature with no additional tuning parameters (apart from deforming the edge shape). In contrast, an impurity is inherently tunable as both the sign as well as the amplitude of the impurity potential can be varied. This allows for tunability of the response. For example, the direction of the current can be switched by simply changing the sign of the potential.

V. RESPONSE TO MULTIPLE IMPURITIES

We next consider the response to multiple impurities.

A. Correlated disorder

We first take up the case of correlated impurities, as defined in Eq. 4. As discussed in the previous section, each impurity induces a local current loop whose chirality is determined by the sign of the impurity potential. As all impurities are of the same sign, we have many current loops with the same chirality. As a result, where

impurities are close to one another, their currents fuse to form a larger loop as depicted in Fig. 3(left).

The fusing of current loops leads to observable macroscopic consequences. In Fig. 4, we show physical properties for two disorder realizations with concentrations $\eta = 0.05$ and $\eta = 0.2$. As the order parameters are complex scalars, we write them as $\Delta_{x/y}^j = |\Delta_{x/y}^j| e^{i\theta_{x/y}^j}$, where j is a site index and the $\theta_{x/y}^j$ is the order parameter phase. In the panels on the left, we show the amplitudes of the order parameters, $|\Delta_x|$ and $|\Delta_y|$. We see that impurities locally suppress the amplitudes of both Δ_x and Δ_y components. This is a consequence of the positive sign of the impurity potential. When the negative sign is used, we see local enhancement of order parameters. In the third panel, we plot $\sin(\theta_x - \theta_y)$. Here, θ_x is the phase of Δ_x while θ_y is that of Δ_y . The sine of the difference in angles is a measure of chirality. In the $\Delta_x \pm i\Delta_y$ states, we expect $(\theta_x - \theta_y) = \pm\pi/2$. The sine of this quantity takes the value of ± 1 , serving as an indicator of chirality. In the figure, we see that chirality is robust to impurities. Within the parameter regime that we have explored, we do not see any domain walls separating regions of differing chirality.

In the fourth column in the figure, we show the spatial distribution of the magnetic field. At low impurity concentration, we see localized (negative) magnetic fields around each impurity. At larger impurity concentrations, these field regions come closer to one another. In the figure, for the two concentrations shown, we see field distributions that are skewed towards negative values. This is tied to the sign of W , the impurity potential. The spread is set by the magnitude W , the strength of each impurity potential, as well as the concentration, η . This field distribution is a measurable signature of impurities that can be accessed by probes such as NV centres.

B. Random disorder

We next consider disorder with random sign as given by Eq. 5. Here, impurity-generated current loops have random chiralities. As shown in Fig. 3(right), this leads to incoherent currents with no loop structure. We obtain strong local currents in random directions. In Fig. 5, we show physical properties that arise from random disorder. In the left two panels, we show the amplitudes of the order parameters. The impurities suppress the amplitudes in some regions and enhance them in others. This is to be contrasted with the case of correlated impurities where the order parameter is either suppressed or enhanced, but not both simultaneously. The amplitude changes in Δ_x as well as in Δ_y are correlated as they arise from the same impurities. In the third panel, we plot $\sin(\theta_x - \theta_y)$, an indicator of chirality as described above. The chirality remains robust with no sign of domain formation.

The fourth column depicts the induced magnetic flux. Each impurity gives rise to a local flux, with the flux

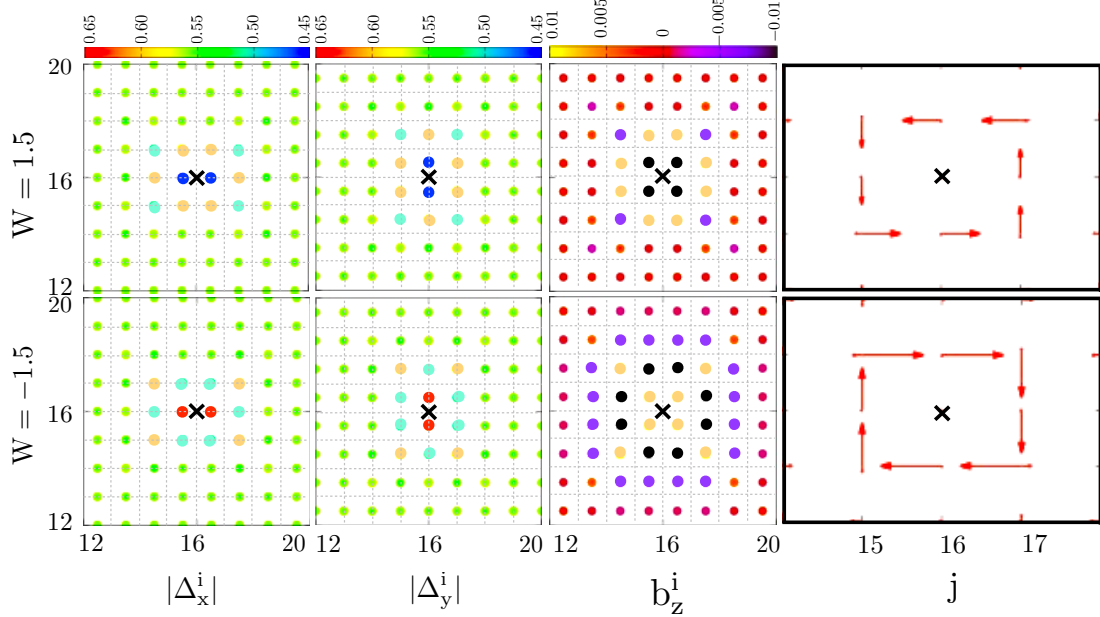


FIG. 1: (Colour online) Response to a single impurity corresponding to a positive (top panels) and a negative (bottom panels) on-site potential. The data have been calculated for $g = 4t$ with the impurity position indicated by an ‘x’. The chirality in all panels is of the $\Delta_x + i\Delta_y$ type. The panels show the order parameter on the x-bonds, those on the y-bonds, the magnetic field through each plaquette and the induced bond currents.

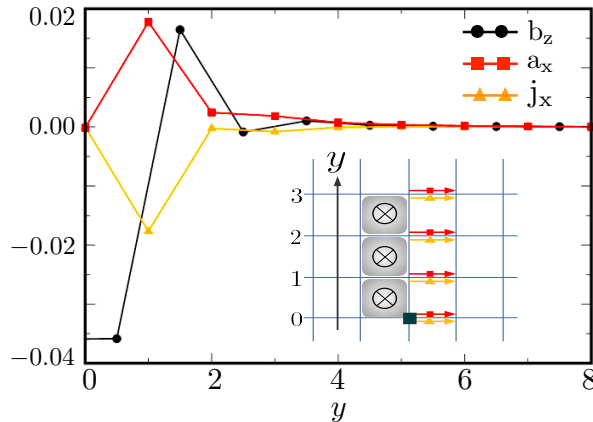


FIG. 2: (Colour online) Response to a single impurity. Profiles of induced current, vector potential and magnetic field for $W = 3.5t$ and $g = 4t$. In the enclosed cartoon, the impurity location is shown as a dark square. This point is taken to be $(0, 0)$. The current and vector potential are shown along bonds parallel to the x -axis at various values of y . The field shown is on plaquettes at various y values.

direction fixed by the sign of the impurity. Away from impurities, the flux is close to zero. Around a positive or negative impurity, the flux takes a negative or positive value respectively. This leads to a broad distribution

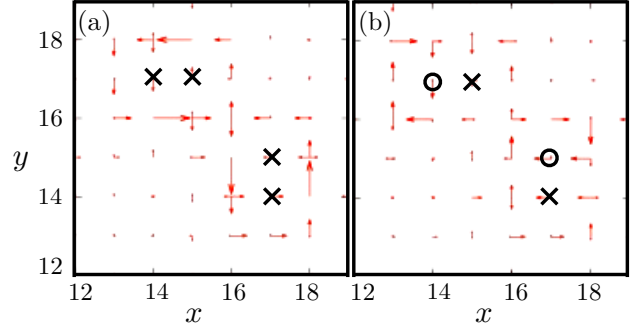


FIG. 3: (Colour online) Currents with proximate impurities. In (a), all impurities have the same sign. Their positions are labelled with ‘x’. In (b), impurities have mixed sign, indicated using ‘x’ and ‘o’.

that is roughly equally spread on either side of zero. The width of the distribution is set by W , the strength of the impurity potential, as well as η , the impurity concentration.

C. Comparing field distributions

We focus on magnetic field distributions, as they are particularly suited for measurements by NV centre probes. In Fig. 6, we compare the field distributions gen-

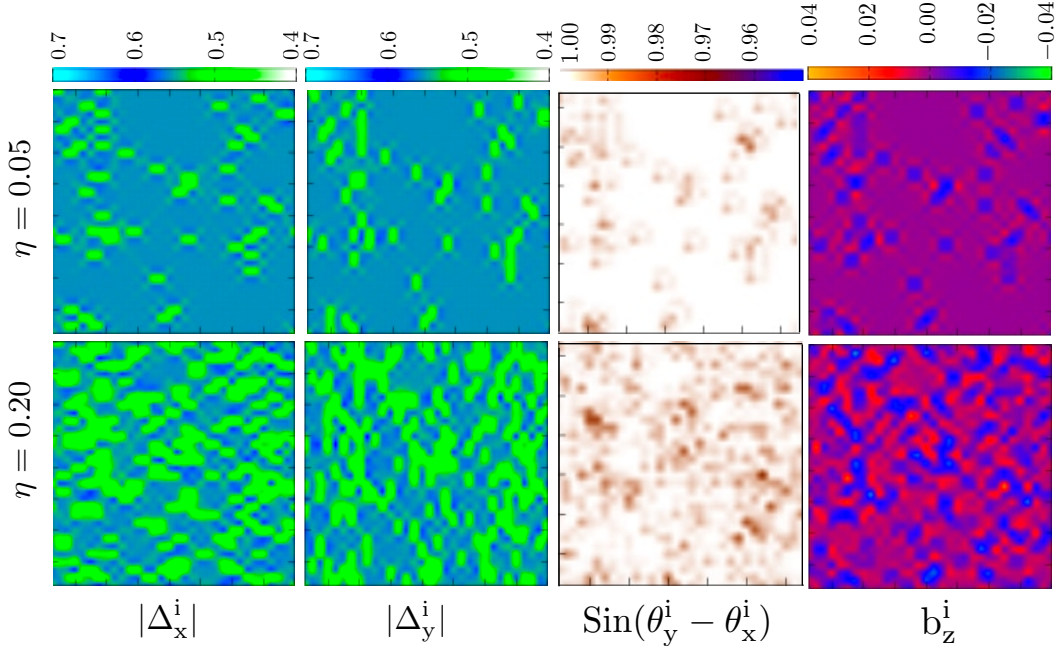


FIG. 4: (Colour online) Response to correlated impurities with $W = 0.5t$ and $g = 4t$ on a 32×32 lattice. We show snapshots for two disorder realizations with concentrations $\eta = 0.05$ and $\eta = 0.2$. From left to right, we show order parameter amplitudes on x bonds, that on y bonds, sine of the phase difference in the two components and finally, the magnetic field.

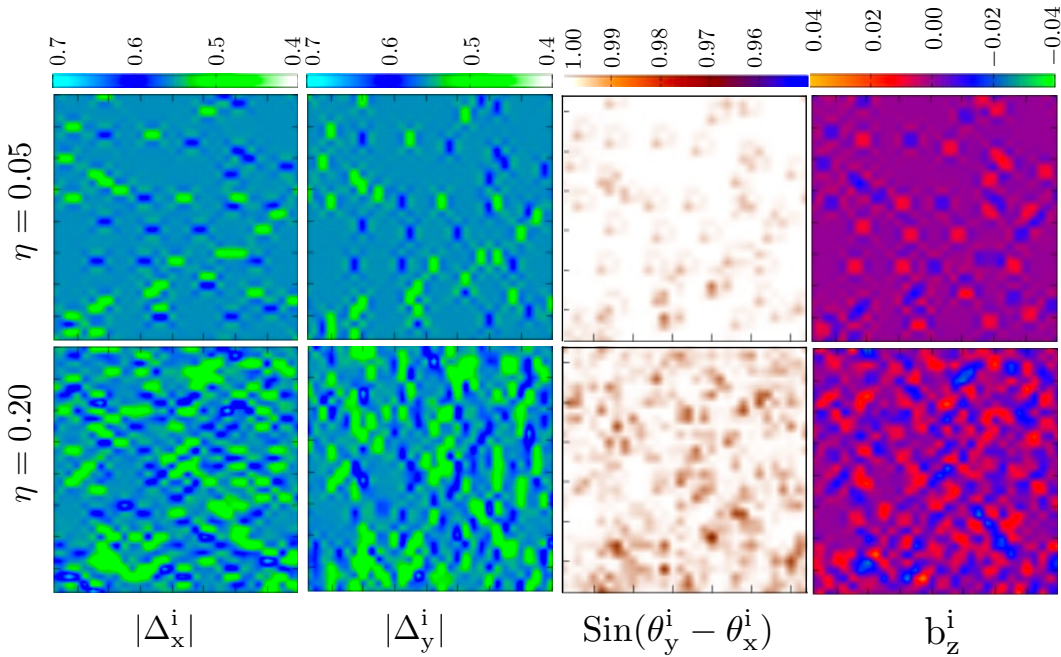


FIG. 5: (Colour online) Response to random impurities. The parameters and the plotted quantities are the same as in Fig. 4.

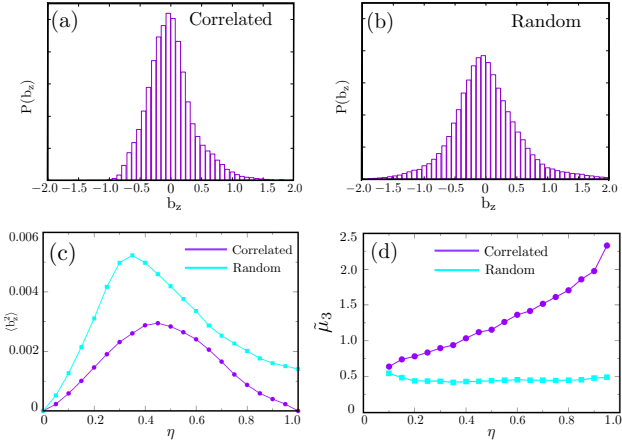


FIG. 6: (Colour online) Magnetic field distributions generated by correlated and random disorder. Histograms of field values are shown in (a) and (b), with the disorder concentration fixed at 20%. (c) The variance of the distributions is shown as a function of disorder concentration. (d) The skewness of the distributions vs. disorder concentration. In all panels, the data corresponds to $g = 4t$, $W = 2t$ and $L = 32$, averaged over 100 disorder realizations.

erated by correlated and random disorder. In panels (a) and (b), we show histograms of field values. In both cases, the mean of the distribution is pinned at zero, i.e., $\langle b_z \rangle = 0$. This is a consequence of periodic boundary conditions, whereby our lattice system forms a torus. As this torus does not enclose a magnetic monopole charge, the net magnetic flux must vanish and the mean of the field distribution must remain zero. Despite having the same mean value, the two field distributions are markedly different.

Correlated disorder creates a skewed distribution as each impurity induces a current loop with the same chirality. The distribution has a longer tail on one side as seen from Fig. 6(a). This reflects a bias towards one magnetic field direction over the other. In contrast, random disorder leads to local currents with both chiralities. This leads to a nearly symmetric field distribution centred at zero. The distribution is wider than in the correlated case. This is a consequence of having strong local currents when impurities with opposite signs are in close proximity. These lead to localized regions with strong fields. Such regions can correspond to either of the two field directions.

We compare quantitative measures of these distributions in panels (c) and (d). Random disorder leads to a higher variance for any disorder concentration. This reflects a wider spread of field values and a broader histogram. This can be visually seen by comparing the histograms in panels (b) and (a). In panel (c), we see the variance in the field distribution changes non-monotonically with disorder concentration. This is because strong disorder suppresses order parameter amplitudes and, in turn, the supercurrents in the sample.

We next compare the skewness of the distributions, defined as $\tilde{\mu}_3 = E[\{(X - \mu)/\sigma\}^3]$. This quantifies the asymmetry of the distribution about the mean. As seen in Fig. 6(d), correlated disorder leads to significantly higher skewness for any value of the impurity concentration. In the random case, the skewness is small but non-zero. This reflects an inherent bias in the system that arises from the chirality of the ground state. In other words, there is a small preference for current loops of chirality over another. However, this is a much weaker effect than that induced by correlations in disorder.

Measurements with NV centres are particularly suited to finding statistical properties of field distributions. With adatoms on a candidate material, these measurements can reveal the character of the underlying superconductor. In particular, the contrast between random and correlated disorder serves as a clear signature of chiral superconductivity.

VI. DISCUSSION

A fascinating consequence of chiral superconductivity is the presence of persistent currents along the sample edge. Despite sustained efforts over decades, such currents have not been observed in experiments. We discuss an alternative in the form of disorder-induced current. Our results show that (a) impurities generically induce local currents in a chiral superconductor and (b) correlated disorder can lead to long ranged currents within the sample. These properties offer significant advantages. In an edge current setup, the bulk chirality serves as a biasing field that drives a current. This bias is in-built and not tunable. In contrast, a disorder potential provides an ‘external’ biasing field that is both tunable and flipable. This allows for disorder-currents to be tunable in orientation, strength and in spatial extent. As a general principle, currents driven by an external biasing field are significantly easier to detect. This is exemplified by the recent detection of an edge current in MoTe₂⁵, where an external current was used to drive a current.

Our analysis is based on a toy model for chiral $p_x \pm ip_y$ superconductivity on a square lattice. However, our results are not model-dependent. Rather, they reflect a generic symmetry-allowed phenomenon – an impurity in a chiral (quasi-)two-dimensional system gives rise to a localized circulating current. Indeed, such a current has been reported in an earlier study on impurity response in a chiral superconductor²⁸. The same physics has also been seen in a Chern insulator, a non-superconducting phase that breaks time-reversal symmetry²⁷. These developments can be traced to studies on integer quantum Hall systems with plateau-shaped potentials²⁹. Going beyond single impurities, we have discussed current signatures in the case of multiple impurities. Correlations in disorder manifest as correlations in the induced magnetic field, giving rise to more complex signatures of chirality.

We have used an improved Bogoliubov-deGennes

scheme³⁰ in our calculations, where the order parameters *and* the vector potential are determined self-consistently. As far as we are aware, this has only been achieved previously in certain simple cases that are amenable to semi-analytic methods. A classic example is the calculation of the profile of a single vortex in a superconductor³¹. A second, more pertinent, example is edge current in the context of Sr_2RuO_4 ²⁶. In both these examples, symmetry reduces the vector potential and the order parameter into functions of one variable. Both can be calculated self-consistently in this effective one-dimensional problem. However, this approach cannot be extended beyond such idealized cases. Our algorithm, based on Eq. 10, is suitable for a wider array of problems. For example, it can be used to determine field distributions in vortices and vortex lattices.

Our approach complements earlier studies on impurities in chiral superconductors. In particular, Refs. 32 and 33 present detailed studies of impurity-induced in-gap states. They further discuss periodic arrangements of

impurities, where bound states hybridize to form bands that can have topological character. Here, we do not focus on bound states or quasiparticle bands. Rather, we discuss currents induced in the superconducting ground state and in turn, the magnetic fields that they generate. In the discussion above, we have restricted our attention to weak disorder and zero temperature, a situation in which impurity-induced bound states do not play a role. In future studies on realistic systems, their effects can be taken into account. Impurity-currents in a chiral superconductor have been previously discussed in Ref. 28. Our results can be viewed as an extension where the magnetic field has been determined with due care.

We have used two disorder schemes as described by Eqs. 4 and 5. These schemes are inspired by studies of impurities³⁴ and adatoms. In several contexts, adatoms have been shown to bring out interesting properties. For instance, adatoms on graphene have been shown to give rise to superconductivity^{35,36}.

-
- * Electronic address: madhuparna.k@gmail.com
- † Electronic address: ganesh@imsc.res.in
- ¹ C. Kallin and J. Berlinsky, *Reports on Progress in Physics* **79**, 054502 (2016).
- ² K. I. Wysokiński, *Condensed Matter* **4** (2019), 10.3390/condmat4020047.
- ³ A. Leggett, M. Leggett, and O. U. Press, *Quantum Liquids: Bose Condensation and Cooper Pairing in Condensed-matter Systems*, Oxford Graduate Texts (OUP Oxford, 2006).
- ⁴ K. C. Nowack, E. M. Spanton, M. Baenninger, M. König, J. R. Kirtley, B. Kalisky, C. Ames, P. Leubner, C. Brüne, H. Buhmann, L. W. Molenkamp, D. Goldhaber-Gordon, and K. A. Moler, *Nature Materials* **12**, 787 (2013).
- ⁵ W. Wang, S. Kim, M. Liu, F. A. Cevallos, R. J. Cava, and N. P. Ong, *Science* **368**, 534 (2020).
- ⁶ A. J. Leggett and Y. Liu, “Symmetry properties of superconducting order parameter in Sr_2RuO_4 ,” (2020), [arXiv:2010.15220 \[cond-mat.supr-con\]](https://arxiv.org/abs/2010.15220).
- ⁷ Y. Maeno, S. Kittaka, T. Nomura, S. Yonezawa, and K. Ishida, *Journal of the Physical Society of Japan* **81**, 011009 (2012), <https://doi.org/10.1143/JPSJ.81.011009>.
- ⁸ P. K. Biswas, H. Luetkens, T. Neupert, T. Stürzer, C. Baines, G. Pascua, A. P. Schnyder, M. H. Fischer, J. Goryo, M. R. Lees, H. Maeter, F. Brückner, H.-H. Klauss, M. Nicklas, P. J. Baker, A. D. Hillier, M. Sigrist, A. Amato, and D. Johrendt, *Phys. Rev. B* **87**, 180503 (2013).
- ⁹ R. Nandkishore, L. S. Levitov, and A. V. Chubukov, *Nature Physics* **8**, 158 (2012), [arXiv:1107.1903 \[cond-mat.mes-hall\]](https://arxiv.org/abs/1107.1903).
- ¹⁰ A. M. Black-Schaffer and C. Honerkamp, *Journal of Physics: Condensed Matter* **26**, 423201 (2014).
- ¹¹ Y.-T. Hsu, A. Vaezi, M. H. Fischer, and E.-A. Kim, *Nature Communications* **8**, 14985 (2017), [arXiv:1606.00857 \[cond-mat.supr-con\]](https://arxiv.org/abs/1606.00857).
- ¹² R. Ganesh, G. Baskaran, J. van den Brink, and D. V. Efremov, *Phys. Rev. Lett.* **113**, 177001 (2014).

- ¹³ L. Jiao, S. Howard, S. Ran, Z. Wang, J. O. Rodriguez, M. Sigrist, Z. Wang, N. P. Butch, and V. Madhavan, *Nature* **579**, 523 (2020).
- ¹⁴ J. R. Kirtley, C. Kallin, C. W. Hicks, E.-A. Kim, Y. Liu, K. A. Moler, Y. Maeno, and K. D. Nelson, *Phys. Rev. B* **76**, 014526 (2007).
- ¹⁵ C. W. Hicks, J. R. Kirtley, T. M. Lippman, N. C. Koshnick, M. E. Huber, Y. Maeno, W. M. Yuhasz, M. B. Maple, and K. A. Moler, *Phys. Rev. B* **81**, 214501 (2010).
- ¹⁶ F. Casola, T. van der Sar, and A. Yacoby, *Nature Reviews Materials* **3**, 17088 (2018), [arXiv:1804.08742 \[cond-mat.str-el\]](https://arxiv.org/abs/1804.08742).
- ¹⁷ J.-P. Tetienne, N. Dotschuk, D. A. Broadway, A. Stacey, D. A. Simpson, and L. C. L. Hollenberg, *Science Advances* **3** (2017), 10.1126/sciadv.1602429, <https://advances.sciencemag.org/content/3/4/e1602429.full.pdf>.
- ¹⁸ M. J. H. Ku, T. X. Zhou, Q. Li, Y. J. Shin, J. K. Shi, C. Burch, L. E. Anderson, A. T. Pierce, Y. Xie, A. Hamo, U. Vool, H. Zhang, F. Casola, T. Taniguchi, K. Watanabe, M. M. Fogler, P. Kim, A. Yacoby, and R. L. Walsworth, *Nature (London)* **583**, 537 (2020), [arXiv:1905.10791 \[cond-mat.mes-hall\]](https://arxiv.org/abs/1905.10791).
- ¹⁹ A. Marguerite, J. Birkbeck, A. Aharon-Steinberg, D. Halbertal, K. Bagani, I. Marcus, Y. Myasoedov, A. K. Geim, D. J. Perello, and E. Zeldov, *Nature* **575**, 628 (2019).
- ²⁰ P. E. C. Ashby and C. Kallin, *Phys. Rev. B* **79**, 224509 (2009).
- ²¹ S. Lederer, W. Huang, E. Taylor, S. Raghu, and C. Kallin, *Phys. Rev. B* **90**, 134521 (2014).
- ²² Y. Imai, K. Wakabayashi, and M. Sigrist, *Phys. Rev. B* **85**, 174532 (2012).
- ²³ N. B. Clara, *Intrinsic Topological Superconductors with Triplet Pairing*, Master’s thesis, University of Copenhagen (2017).
- ²⁴ D. J. Scalapino, S. R. White, and S. Zhang, *Phys. Rev. B* **47**, 7995 (1993).
- ²⁵ M. Matsumoto and M. Sigrist, *Journal of the*

- Physical Society of Japan **68**, 994 (1999), <https://doi.org/10.1143/JPSJ.68.994>.
- ²⁶ A. Furusaki, M. Matsumoto, and M. Sigrist, Phys. Rev. B **64**, 054514 (2001).
- ²⁷ V. B. Jha, G. Rani, and R. Ganesh, Phys. Rev. B **95**, 115434 (2017).
- ²⁸ Y.-W. Guo, W. Li, and Y. Chen, Frontiers of Physics **12** (2017), 10.1007/s11467-017-0683-9.
- ²⁹ C. J. B. Ford, P. J. Simpson, I. Zailer, D. R. Mace, M. Yosefin, M. Pepper, D. A. Ritchie, J. E. F. Frost, M. P. Grimshaw, and G. A. C. Jones, Phys. Rev. B **49**, 17456 (1994).
- ³⁰ J. Zhu, *Bogoliubov-de Gennes Method and Its Applications*, Lecture Notes in Physics (Springer International Publishing, 2016).
- ³¹ M. Tinkham, *Introduction to Superconductivity*, Dover Books on Physics Series (Dover Publications, 2004).
- ³² V. Kaladzhyan, J. Röntynen, P. Simon, and T. Ojanen, Phys. Rev. B **94**, 060505 (2016).
- ³³ A. Kreisel, T. Hyart, and B. Rosenow, “Tunable topological states hosted by unconventional superconductors with adatoms,” (2021), arXiv:2102.12502 [cond-mat.supr-con].
- ³⁴ A. V. Balatsky, I. Vekhter, and J.-X. Zhu, Rev. Mod. Phys. **78**, 373 (2006).
- ³⁵ G. Profeta, M. Calandra, and F. Mauri, Nature Physics **8**, 131 (2012).
- ³⁶ B. M. Ludbrook, G. Levy, P. Nigge, M. Zonno, M. Schneider, D. J. Dvorak, C. N. Veenstra, S. Zhdanovich, D. Wong, P. Dosanjh, C. Straßer, A. Stöhr, S. Forti, C. R. Ast, U. Starke, and A. Damascelli, Proceedings of the National Academy of Sciences **112**, 11795 (2015), <https://www.pnas.org/content/112/38/11795.full.pdf>.